

# Determination of Electrochemical Performance and Thermo-Mechanical-Chemical Stability of SOFCs from Defect Modeling

Eric D. Wachsman  
 Department of Materials  
 Science and Engineering  
 University of Florida  
 Gainesville, FL 32611-6400  
 (352) 846-2991  
 ewach@mse.ufl.edu



Don Collins  
 (304) 285-4156  
 Donald.Collins@netl.doe.gov

## Objectives

- Advance the fundamental understanding of the continuum-level electrochemistry of oxide mixed ionic-electronic conductors in relation to their performance in SOFCs.
- Express this understanding in a mathematical framework.
- Produce software modules containing relevant formulae of the continuum-level electrochemical model for incorporation into SOFC failure analysis software used by NETL, PNNL, ORNL and the SECA industrial teams.
- Obtain fundamental constants (defect diffusivities, equilibrium and time constants), required for implementing the continuum-level electrochemical model, from experiment.
- Verify the continuum-level electrochemical model through experiment in *transient* and *steady state* conditions.

## Key Milestones

- Complete the continuum-level electrochemical model for *steady state* conditions, using potential dependent boundary conditions and without assuming a linear Galvani potential.
- Complete the continuum-level electrochemical model for *transient* conditions, using potential dependent boundary conditions and assuming a linear Galvani potential.
- Compile software modules for vacancy concentration and electron concentration in *n*-type and *p*-type mixed ionic-electronic conductors.
- Extend the continuum-level electrochemical model to thermo-mechanical and thermo-chemical properties of mixed ionic-electronic conductors.
- Measure time constants for degradation/failure mechanisms in conventional SOFCs.
- Measure time constants for transport processes in LSM/zirconia/LSM symmetric cells.

## Approach

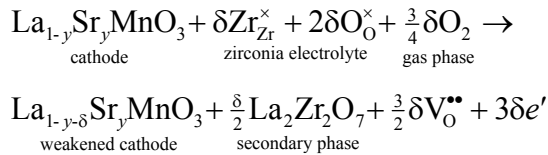
Mixed ionic-electronic conductors (MIECs) (including pure ionic, electronic conductors) are currently being studied for potential application in solid oxide fuel cells (SOFCs) as electrolytes, interconnects and electrodes [1]. Despite the success achieved in engineering SOFCs, their full potential has yet to be realized because of certain problems. In broad terms, these problems include efficiency losses, thermo-mechanical stability and chemical stability.

The electrochemical efficiency of SOFC components largely depends on two related factors: bulk and interfacial transport of charge carriers. For bulk transport, the *ideal* electrolyte has high ionic and negligible electronic conductivity; the *ideal* electrode has high ionic and high electronic conductivity; and the *ideal* interconnect has

negligible ionic and high electronic conductivity.

Thermo-mechanical stability includes several aspects of the SOFC that relate temperature and the elastic properties of the MIEC. Perhaps the most pertinent of these, however, is thermal cycling, which is concerned with the mechanical stresses and strains that result from repeated heating and cooling. This is a critical feature for any practical device, because one must determine if it can survive thermal cycles that are inherent to its operation and application.

The chemical stability of the SOFC components concerns largely deleterious chemical reactions between the SOFC components. Both are dependent on the concentration of point defects. An example of the latter is (at typical SOFC operating temperatures) the reaction between cubic-stabilized zirconia (CSZ) electrolytes and lanthanum strontium manganate (LSM) cathodes, which occurs as follows:



which shows explicitly that the presence of charge carriers (oxygen vacancies and electrons as written) plays a vital role in the formation of lanthanum zirconate from CSZ and LSM.

Our approach to resolving the issues of efficiency losses, thermo-mechanical and thermo-chemical stability is threefold. The first is developing a fundamental understanding, including a mathematical description, of the thermodynamics and transport of defects in MIECs in fuel cell conditions (i.e., in chemical and electrical potential gradients). The second is relating this understanding to the relevant material properties of the MIECs. Finally, the first two components must be made available in a useful form (e.g., software modules), to research teams for implementation into their failure analysis models for SOFC stacks.

The continuum-level electrochemical model we have developed includes defect thermodynamics and transport (derived from the Nernst-Planck flux equation). Here defect thermodynamics concerns defect concentration dependence on  $P_{\text{O}_2}$ . The usual method is to

solve a system of equations consisting of mass action equations from the defect equilibria and a charge balance equation (and, if necessary, mass and site balance equations) for defect species. However, depending on the defect species involved, the system of equations can result in high order ( $> 3$ ) polynomials [2] with no analytical solution. The traditional way of simplifying these equations is the Brouwer method, which examines the equilibria in separate Brouwer regimes in which only two defect species dominate [3]. This method is quite successful in generating the general form of defect equilibrium diagrams. However, it produces formulae that are discontinuous across the Brouwer regimes. This is a problem for some MIECs in a  $P_{\text{O}_2}$  gradient where the defect equilibria span more than one regime. Moreover, an electrical potential can drive an MIEC from one regime to the next. Conversely, by considering three defects instead of two, we have derived equations that are continuous across at least two regimes. These are given below for  $n$ -type oxide MIECs such as samaria-doped ceria (SDC),

$$c_v(P_{\text{O}_2}) = \left[ \frac{3}{4} K_r^{\frac{1}{2}} P_{\text{O}_2}^{-\frac{1}{4}} + \left( \frac{1}{2} c_A \right)^{\frac{3}{2}} \right]^{\frac{2}{3}}$$

and

$$c_e(P_{\text{O}_2}) = K_r^{\frac{1}{2}} P_{\text{O}_2}^{-\frac{1}{4}} \left[ \frac{3}{4} K_r^{\frac{1}{2}} P_{\text{O}_2}^{-\frac{1}{4}} + \left( \frac{1}{2} c_A \right)^{\frac{3}{2}} \right]^{-\frac{1}{3}} \quad (1)$$

where  $c_v$ ,  $c_e$ , and  $c_A$  are the concentration of vacancies, electrons and acceptor dopant, respectively.  $K_r$  is the equilibrium constant for the oxygen exchange reaction between the oxide and gaseous  $\text{O}_2$ . Details of the derivation may be found in Reference 4.

To model defect transport in MIECs we solved the Nernst-Planck, material balance, and current density equations

$$j_i = -D_i \nabla c_i - u_i c_i \nabla \phi \quad (2)$$

Nernst-Planck

$$\frac{\partial c_i}{\partial t} = -\nabla j_i + \Gamma_i$$

material balance

$$J = q \sum_i z_i j_i$$

current density

where  $j$  is flux density,  $J$  is current density,  $D$  is diffusivity,  $c$  is concentration,  $u$  is electrical mobility,  $t$  is time,  $\Gamma$  is the rate of formation of defect species due to homogenous chemical reactions,  $\phi$  is the Galvani potential,  $\zeta$  is charge equivalence,  $q$  is the elementary electronic charge,  $k_B$  is Boltzman's constant,  $T$  is temperature and the subscript "i" refers to the  $i$ th defect species.

In steady state conditions, the solutions, for  $n$ -type MIECs, include

$$c_V(x) - c_{V_0} - \frac{(D_V \gamma - j_V) c_A}{z_V (z_V - z_e) D_V \gamma} \cdot \ln \frac{z_V (z_V - z_e) D_V \gamma c_V(x) - j_V c_A}{z_V (z_V - z_e) D_V \gamma c_{V_0} - j_V c_A} = -\gamma x \quad (3)$$

$$\phi(x) = \phi_0 - \frac{(D_V \gamma - j_V) k_B T}{z_V q D_V \gamma} \cdot \ln \frac{z_V (z_V - z_e) D_V \gamma c_V(x) - j_V c_A}{z_V (z_V - z_e) D_V \gamma c_{V_0} - j_V c_A} \quad (4)$$

where

$$\gamma = \frac{\Delta \phi}{\lambda L} - \frac{c_{V_L} - c_{V_0}}{L} = -k_B T \frac{z_V u_e j_V - u_V j_e}{z_V (z_V - z_e) q D_e D_V} \quad (5)$$

and  $L$  is the thickness of the MIEC and  $\bar{t}_{ion}$  is the average (necessary when concentration gradients are present) ionic transference number. The subscripts 0 and L refer to the boundary values of the MIEC (i.e., at  $x = 0$  (the anode side) and  $x = L$  (the cathode side)). Also, from the local equilibrium approximation [5],

$\Delta \phi = \Phi_{ext} - \Phi_{th} - k_B T z_V^{-1} q^{-1} \ln(c_{V_L}/c_{V_0})$  and from an SOFC equivalent circuit [5],  $\bar{t}_{ion} \Phi_{th} = \eta + \Phi_{ext}$ ; where  $\Phi_{ext}$  is the potential across the load resistance and  $\Phi_{th}$  is the theoretical/Nernst potential and  $\eta$  is the cell overpotential.

To obtain solutions in transient conditions, we assumed a linear potential distribution. This assumption is best applied to predominantly ionic conductors (e.g., yttria-stabilized zirconia, (YSZ)) or predominantly electronic conductors (e.g., LSM). The results of our transient model (for YSZ) are as follows:

$$c_e(x, t) = \sum_{n=1}^{\infty} b_n e^{-\sqrt{D_e} (n/L)^2 t} \sin n\pi x/L + (c_{e,L}^{\infty} - c_{e,0}^{\infty}) x/L + c_{e,0}^{\infty} \quad (6)$$

$$\phi(x, t) = -z_e D_e u_V^{-1} c_A^{-1} \sum_{n=1}^{\infty} b_n e^{-\sqrt{D_e} (n/L)^2 t} \sin n\pi x/L + (\phi_L^{\infty} - \phi_0^{\infty}) x/L + \phi_0^{\infty} \quad (7)$$

where  $n$  is a positive integer and  $b_n$  is the  $n$ th constant coefficient.  $b_n$  is obtained from the initial and final conditions of the system. The superscript "∞" refers to steady state (final) values.

For both transient and steady state models, *potential-dependent* boundary conditions were obtained by using  $-k_B T \ln K_r = \Delta G_r^{oc} - q\eta$  at the anode and  $-k_B T \ln K_r = \Delta G_r^{oc} + q\eta$  at the cathode; where  $\Delta G_r^{oc}$  is the free energy for the oxygen exchange reaction in *open-circuit* conditions.

Now that we have a model for the thermodynamics and transport of defects in an MIEC, we next seek to relate it to SOFC performance and material properties of SOFC components. In this work we consider current and power efficiency, power density and elastic modulus.

The current efficiency and power efficiency of an SOFC is given by

$$\zeta_J(\Delta \phi) = J/J_V \text{ and } \zeta_P(\Delta \phi) = J\Phi_{ext}/(J_V \Phi_{th}) \quad (8)$$

while the power density can be obtained from Equations (2) through (5) since power,  $\dot{W} = J\Phi_{ext}$ .

The bond energy,  $E$ , between atoms in a crystal, may be approximated by  $E = A/r^n - B/r^m$  [6], where  $r$  is the interatomic distance, and  $A$ ,  $B$ ,  $n$  and  $m$  are empirically determined constants ( $m < n$ ). The elastic modulus for a perfect crystal,  $Y \approx 1/r_0(d^2E/dr^2)_{r=r_0}$ . The lattice constant,  $a \propto r_0$  and  $a$  increases almost linearly with  $c_V$  [7, 8]. Therefore,  $Y$  may be written as follows:

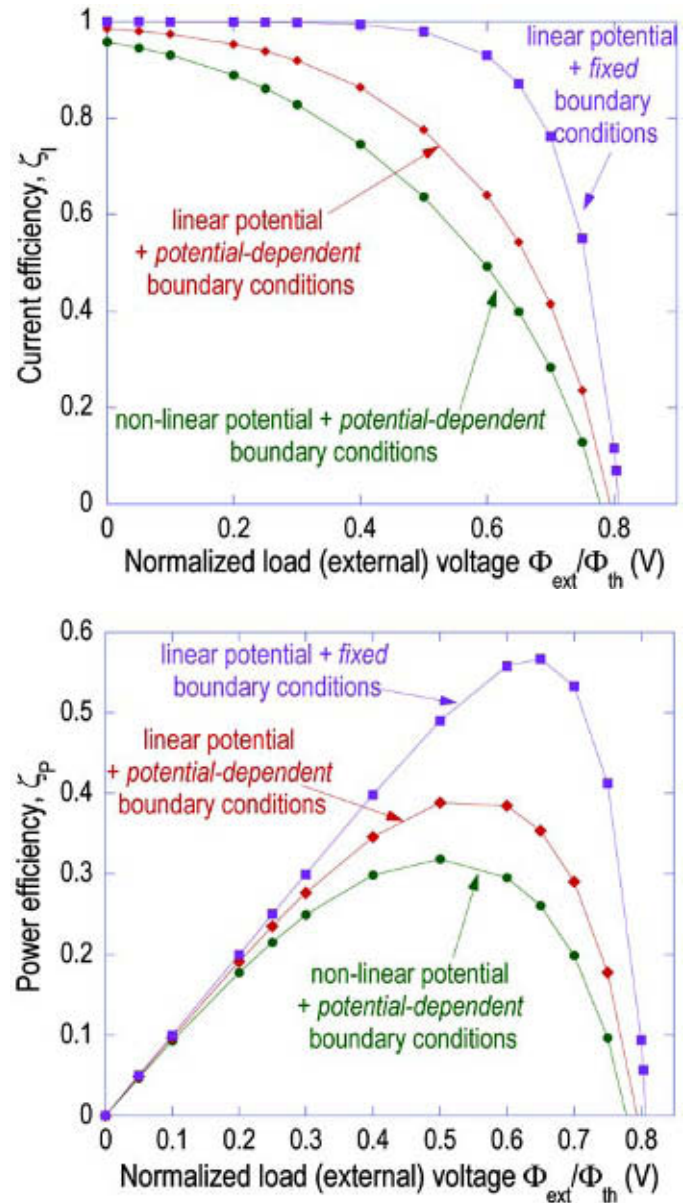
$$Y(x) \approx Y^* (\theta c_V(x) + 1)^{-(m+3)} \quad (10)$$

where  $\theta$  is an empirically determined constant (a function of  $A$ ,  $B$ ,  $n$ , and  $m$ ), and the superscript “\*” refers to stoichiometric conditions (i.e., when  $c_V = 0$ ). The results of the continuum electrochemical model for these properties and the transient response of the concentration distribution are discussed in the next section.

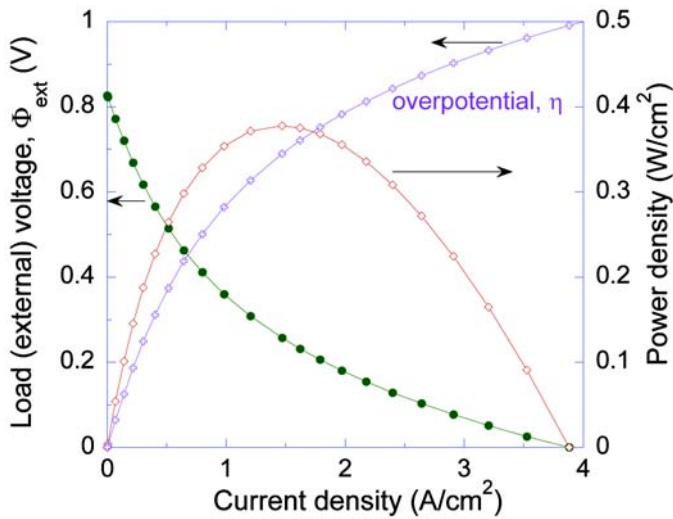
## Results

Figure 1 shows a comparison of current and power efficiencies calculated from models with different assumptions for a doped ceria electrolyte. The figure shows that using fixed boundary conditions and assuming a linear Galvani potential leads to an overestimation of both current and power efficiencies. Assuming a linear potential ignores the efficiency-sapping effects of mixed conduction and using fixed (i.e., independent of potential) boundary concentrations reduces the effects of changing concentration gradients. Consequently, when these assumptions are removed the calculated efficiencies are smaller. These results emphasize the importance of using the correct electrochemical model as the basis for computation of relevant properties.

Figure 2 shows the projected I-V characteristics, power density, and cell overpotential for an SOFC that includes both ionic and electronic contributions. To do this we chose a single layer MIEC, samaria-doped ceria. Though the calculations do not include the electrode resistance or concentration overpotential, the results are remarkably similar to those obtained from experiment, in both magnitude and form. Moreover, the figure shows that the continuum-level electrochemical model yields Tafel-like behavior for the cell



**Figure 1.** Comparison of the current and power efficiency from various models for an SOFC with an acceptor-doped ceria electrolyte, at 800 °C.



**Figure 2.** Predicted  $I$ - $V$  characteristics, power density and overpotential from non-linear potential model for an SOFC with a 1 mm thick samaria-doped ceria electrolyte, at 800 °C.

overpotential. More work must be done to include the effect of the electrodes, but this result clearly demonstrates the power and potential of the continuum-level electrochemical model.

Figure 3 shows the results of extending the continuum-level electrochemical model to mechanical properties, such as the elastic modulus,  $Y$ , in this example. The plots show a general degradation of the elastic modulus towards the anode side ( $x=0$ ) of the electrolyte. Moreover, it is seen that the variation in the elastic modulus is much less in open-circuit conditions (smallest concentration gradients [4]), than in short-circuit conditions (steepest concentration gradients [4]). Consequently, for a given value of  $\theta$ , one may expect that the electrolyte grows weaker as more current passes through the cell. We have similarly modeled the fracture toughness,  $K_{IC}$ , and these results imply that fracture is likely to initiate on the anode side of the SOFC.

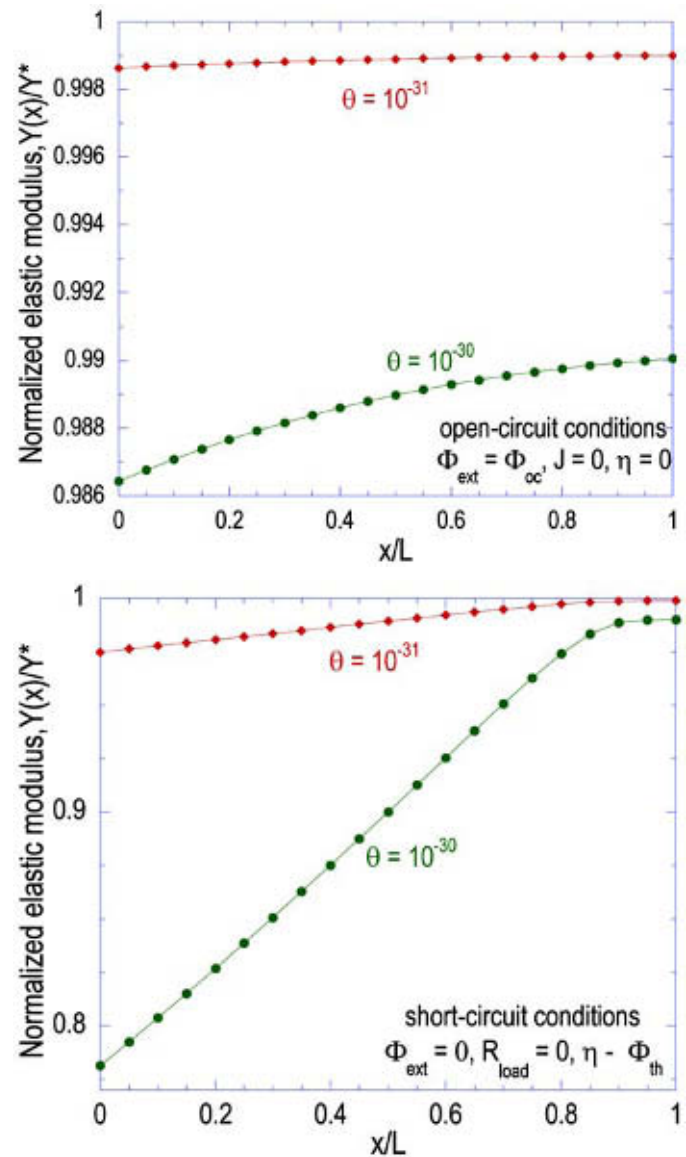


**Figure 3.** Elastic modulus profiles in (a) open-circuit and (b) short-circuit for samaria-doped ceria electrolyte, at 800 °C; anode is at  $x=0$  ( $P_{O_2} = 10^{-20}$  atm), cathode at  $x=L$  ( $P_{O_2} = 0.21$  atm).

Clearly, the continuum-level electrochemical model can facilitate the prediction of the thermo-mechanical properties of SOFCs.

Finally, Figure 4 shows the evolution of the electron concentration profiles in a YSZ electrolyte. In Figure 4a, a load (of voltage  $\Phi_{th}/4$ ) is introduced to the SOFC, which was initially ( $t=0$ ) in open-circuit conditions. The results show that while the boundary concentrations are *instantly* established, the concentration in the bulk lag behind, ostensibly limited by electron diffusivity and electrolyte thickness, as shown in Equation (7). In Figure 4b, a load is again introduced to the SOFC, but this time it carries a 60 Hz sinusoidal ripple with it. The effect and presence of the ripple is evident in the plot, which shows an initial response similar to Figure 4a, with the bulk concentration lagging behind the boundary values. However, after about 6 seconds, the lag is no longer evident even though the ripple persists. This is a result of the amplitude and frequency of the ripple. The amplitude is small enough not to cause great changes in the concentration gradient. While the time constant of the electrolyte ( $\sim 4.5$  s) is  $\sim 270$  times the period (reciprocal frequency) of the ripple. Hence, the electrolyte does not have enough time to respond to the ripple in the bulk, and the ripple's effect is seen only at the boundaries.

## References

1. S.C. Singhal, *Solid State Ionics* **135** (2000) 305.
2. F. W. Poulsen, *Solid State Ionics* **129** (2000) 145.
3. H. L. Tuller, *Nonstoichiometric Oxides*, ed. O. Sorensen, Academic, New York, 1981, ch. 6.
4. E. Wachman and K. Duncan, Stable High Conductivity Bilayered Electrolytes for Low Temperature SOFCs, DOE Final Report, Contract No. DE-AC26-99FT40712, 2002.
5. I. Riess, *J. Electrochem. Soc.* **128** (1981) 2077.
6. M. Barsoum, in *Fundamentals of Ceramics* (McGraw-Hill, 1977).
7. D-J. Kim, *J. Amer. Ceram. Soc.* **72** (1989) 1415.
8. Zacatea, L. Minervinia, D. Bradfielda, R. Grimes and K. Sickafus *Solid State Ionics* **128**, (2000) 243.

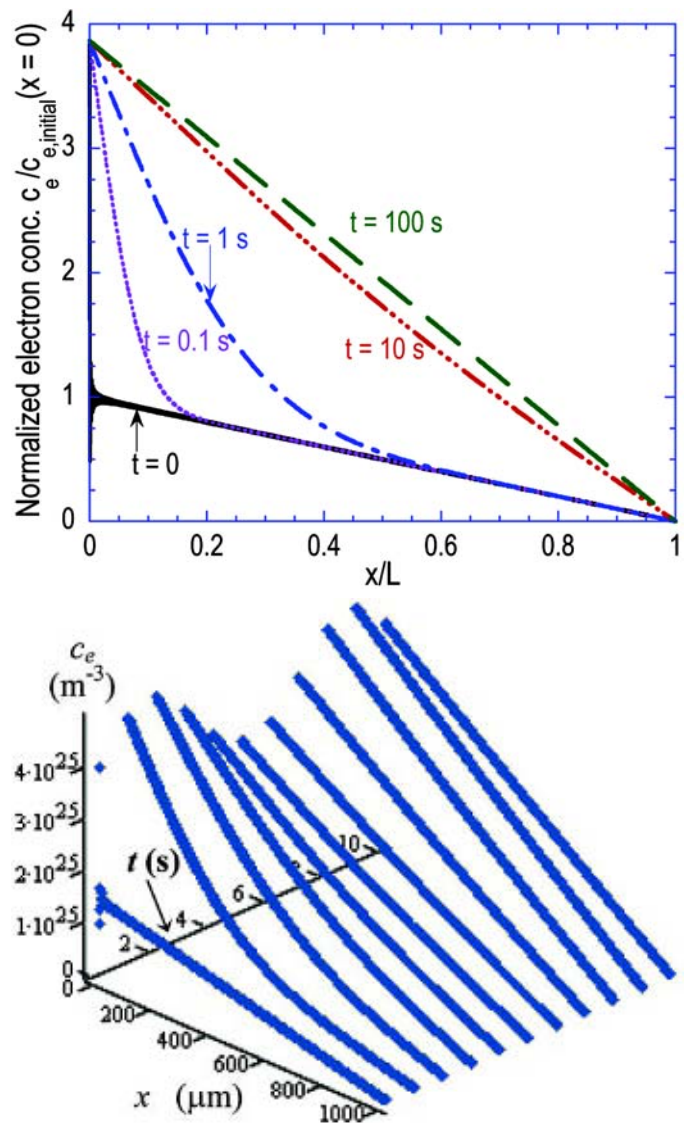


**Figure 4.** Time-dependent evolution of electron concentration profiles in a YSZ electrolyte at 800 °C: (a) load voltage,  $\Phi_{ext}$  goes from open-circuit value to  $\Phi_{th}/4$  (b)  $\Phi_{ext}$  has a 60 Hz sinusoidal ripple; anode is at  $x=0$  ( $P_{O_2} = 10^{-22}$  atm), cathode at  $x=L$  ( $P_{O_2} = 0.21$  atm).